

Article

In Vitro Bio-Testing Comparative Analysis of NiTi Porous Alloys Modified by Heat Treatment

Ekaterina Marchenko , Gulsharat Baigonakova * , Kirill Dubovikov , Oleg Kokorev , Yuri Yasenchuk 
and Alexander Vorozhtsov

Laboratory of Superelastic Biointerfaces, National Research Tomsk State University, 36 Lenin Ave., 634045 Tomsk, Russia; 89138641814@mail.ru (E.M.); kirill_dubovikov@mail.ru (K.D.); kokorevov@yandex.ru (O.K.); yayuri2008@gmail.com (Y.Y.); abv1953@mail.ru (A.V.)

* Correspondence: gat27@mail.ru

Abstract: The present work is aimed at studying the surface cytocompatibility of porous NiTi obtained by self-propagating high temperature synthesis (SHS), and then annealed in air at 500–1000 °C. Using cytotoxicity tests in vitro, it was found that the cells had attached to the oxidized surface in the amount sufficient for their growth and proliferation on the substrate. The surfaces of the annealed samples and the control sample were studied by XRD, SEM and optical microscopy. It was found that there is a correlation between cell hemolysis and nickel-containing phases on the surface. Thus, annealing at 500–700 °C worsens cytocompatibility compared to the control sample, but annealing at 800–1000 °C improves cytocompatibility.

Keywords: porous NiTi alloy; biomaterial; heat treatment; biocompatibility; cytocompatibility



Citation: Marchenko, E.; Baigonakova, G.; Dubovikov, K.; Kokorev, O.; Yasenchuk, Y.; Vorozhtsov, A. In Vitro Bio-Testing Comparative Analysis of NiTi Porous Alloys Modified by Heat Treatment. *Metals* **2022**, *12*, 1006. <https://doi.org/10.3390/met12061006>

Academic Editor: Russell Goodall

Received: 9 May 2022

Accepted: 10 June 2022

Published: 13 June 2022

Publisher's Note: MDPI stays neutral with regard to jurisdictional claims in published maps and institutional affiliations.



Copyright: © 2022 by the authors. Licensee MDPI, Basel, Switzerland. This article is an open access article distributed under the terms and conditions of the Creative Commons Attribution (CC BY) license (<https://creativecommons.org/licenses/by/4.0/>).

1. Introduction

The characteristic properties of titanium nickelide, such as the shape memory effect, superelasticity, high corrosion resistance and damping ability make the alloy highly applicable in various fields of medicine [1–4]. Porous materials are of particular importance due to their integration into biological tissues and long-term functioning in a living organism [5–8]. Firstly, bone tissues grow into the pores of the implant and provide stable fixation. Secondly, the rough surface of the porous implant increases the specific surface area of the interface between the implant and the biological tissue, and reduces the contact loads at the interface.

One of the promising methods in powder metallurgy is self-propagating high-temperature synthesis (SHS), whose advantages are high productivity and economy. In the NiTi implants the SHS method is applied to obtain open interconnected pores which make it possible to transport body fluids together with a new forming tissue through the implant, supporting the growth of the tissue [9,10]. An important advantage of SHS is the formation of a protective layer on the pore surface, which spontaneously forms from oxycarbonitrides and protects the alloy from electrochemical corrosion in chlorine-containing solutions [11–14]. However, the influence of oxidation processes on the phase composition, structure and cytocompatibility of the porous SHS-NiTi during short-term annealing in air has remained insufficiently studied [15]. Due to a larger specific surface area, the annealing process of the porous material occurs faster, which results in the disturbance of the balance between mechanical properties and corrosion resistance.

While being manufactured the implants made of porous NiTi alloys are subjected to short-time heat treatment in the temperature range of 700–1000 °C to give them their individual shapes, which results in structural and phase changes in the surface and near-surface layers, therefore the heat treatment process requires special control. Regarding creating implants for prosthetics of the middle face zone from porous SHS-NiTi plates, the manufacturing technology includes heat treatment in air at temperatures of 700–900 °C [16,17]. The porous SHS-TiNi alloy is used to create endoprostheses of the temporomandibular

joint with rubbing surfaces [16,18,19]. In the case of such endoprostheses with rubbing surfaces [20,21], heat treatment in air is not used. New properties which characterize the annealed surface are important for the biocompatibility of the implant [22–25], as, for example, any change in the chemical composition of an implant affects the protein adsorption [24].

There are a number of studies devoted to the oxidation mechanisms in cast NiTi alloys during annealing [26–29]. It was concluded that within 1 h of heat treatment a multilayer structure, in which the outer layer is TiO₂, the middle layer is represented by nickel-enriched Ni₃Ti and Ni(Ti) phases and the inner layer is B2-NiTi [28,30–32], forms. TiO₂ forming on the surface of NiTi implants acts as a barrier [26–28,31–35] protecting the surrounding tissues from the toxic effect of the nickel ions which tend to leach from the matrix in aggressive body conditions caused by alternating loads. In the literature described above, the oxidation mechanisms of the cast NiTi were studied, but no studies were found to have considered the short-time annealing of porous SHS-NiTi and its effect on the cytotoxicity and hemocompatibility of the alloy.

The novelty of the work lies in considering the positive role of the surface layers of the porous framework during oxidation in air. Oxidation is the result of forced heat treatment in air during the manufacture of implants from porous SHS-TiNi plates. In this study, the optimal temperature ranges of heat treatment in air for porous SHS-TiNi alloys will be established for the first time. Structure studies, electrochemical methods for selective investigation of the surface in porous alloys, the method of cell deposition on the surface of a porous framework and the microscopic study of hemolysis used in this work will make it possible to establish the optimal temperature ranges of heat treatment.

The aim of this work is to study the influence of short-time annealing in the temperature range of 500–1000 °C on the structure, phase composition, cytocompatibility and hemocompatibility of the porous NiTi produced by SHS.

2. Materials and Methods

2.1. Materials

Porous NiTi ingots with a porosity of 65% were obtained by self-propagating high-temperature synthesis (SHS) [36]. Plates 2 mm × 10 mm × 10 mm in size were cut from porous ingots electrical discharge machining. The whole experiment and the methods applied are schematically shown in Figure 1. Annealing was carried out in air in the temperature range of 500–1000 °C. Quartz tubes with samples were placed in a tubular electric resistance furnace after reaching the required temperature in the furnace. The exposure time of the samples was 5 min. The samples were taken out and cooled in air. For convenience, some symbols were introduced where the number indicates the annealing temperature, for example, NiTi500, NiTi600, however, the NiTi25 sample was not annealed, and it is considered as a control sample.

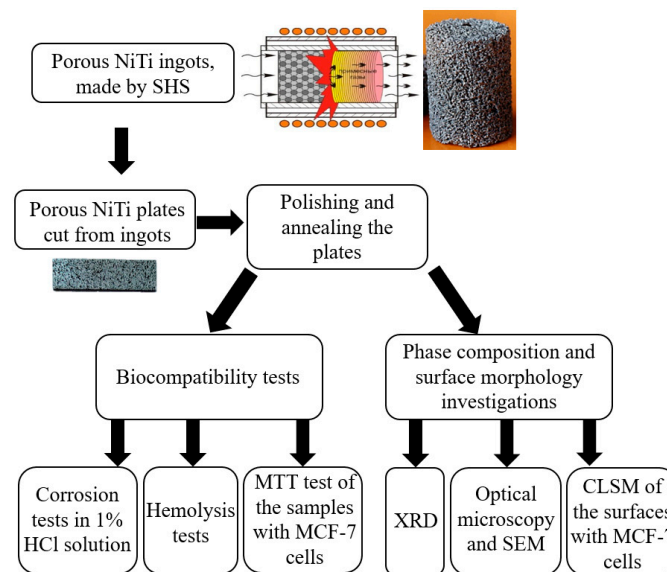


Figure 1. The scheme of the experimental testing.

2.2. Methods

2.2.1. Structural Investigations

The surface phase composition of the samples was studied by XRD in the grazing beam mode using a XRD-6000 diffractometer (Shimadzu, Japan) with CuK- α radiation. To identify the obtained X-ray diffractograms, the crystallography open database (COD) and the materials project web-database and Profex full-profile analysis program were used.

The surface structure of the samples was studied by SEM TESCAN VEGA3 (Tescan, Brno, Czech Republic) and EDS in a secondary electron detection mode and by an optical microscope Axiovert 40 MAT (Carl Zeiss Microscopy GmbH, Jena, Germany).

Fluorescence of the samples from the 10 mm \times 10 mm surface areas was visualized using the LSM-780NLO Confocal Laser Scanning Microscope, Carl Zeiss Microscopy GmbH (Germany). Cells were visualized using double staining with acridine orange and ethidium bromide. Before staining the samples were pre-washed from the medium and flooded with the working dye solution for 10 min. Live cells were stained with acridine orange, and dead cells were stained with ethidium bromide. Fluorescent acridine orange was excited using a laser with a wavelength of 488 nm, and fluorescence was recorded in the range of 495–545 nm. Fluorescent ethidium bromide was excited using a laser with a wavelength of 561 nm, and fluorescence was recorded in the range of 580–690 nm. As a result, fluorescent images of localizations of acridine orange (green) and ethidium bromide (red), and an image obtained in transmitted light mode were superimposed. The number of viable cells was calculated as the arithmetic mean in 3 or 5 view fields of the confocal microscope.

2.2.2. Determination of Ni Content in Solution

The studies were carried out in a 1 mass. % HCl solution after 1800 h of interaction with samples at a temperature of 293 K. During corrosion tests, porous samples 1 mm \times 1 mm \times 10 mm in size were half immersed in test tubes with a solution and hermetically sealed. The tubes were periodically shaken during the entire test period. At certain time intervals, the samples were removed, and the solutions were analyzed under a standard procedure for maintaining the chemical purity of the experimental solutions.

After the samples were extracted from the solutions, the nickel content in those solutions was determined by the colorimetric method using sodium diethyldithiocarbamate. Sodium diethyldithiocarbamate forms a compound with nickel that is easily extractable with isoamyl alcohol. The molar coefficient of light absorption of such a compound is $\xi = 37,000$ at a wavelength of incident radiation $\lambda = 325 \mu\text{m}$. Based on the results of colorimetric measurements of a series of standard solutions, the calibration dependence

of their optical density on the nickel concentration was obtained, from which the nickel concentration in the experimental solutions was determined.

2.2.3. In Vitro Bio-Testing

The annealed samples were washed first in an ultrasonic bath, then with distilled water three times on a shaker for 60 min and autoclaved at 180 °C for one hour. Next, the samples were washed three times with culture medium and placed in the 24-well plate to study cytocompatibility.

2.2.4. Hemolysis Test

Healthy human volunteer donor blood containing sodium citrate (3.8 wt.%) in a ratio of 9:1 was diluted with normal saline (4:5 ratio by volume). Intact and modified NiTi samples were dipped into a standard tube containing 10 mL of normal saline that had been previously incubated at 37 °C for 30 min. Next, 0.2 mL of diluted blood was added to this standard tube and the mixtures were incubated for 60 min at 37 °C. Similarly, normal saline solution was used as a negative control and deionized water as a positive control. After the time period mentioned, all of the tubes were centrifuged for 5 min at 3000 rpm, and the supernatant was carefully removed and transferred to a cuvette for spectroscopic analysis at 545 nm. In addition, hemolysis was calculated using a Uniplan ultraviolet spectrophotometer (Pikon Inc., RF, Tokyo, Japan). Hemolysis percent is the average of three replicates and it is calculated as (Equation (1)):

$$\text{Hemolysis} = \frac{OD_{\text{test}} - OD_{\text{control}}^{\text{negative}}}{OD_{\text{control}}^{\text{positive}} - OD_{\text{control}}^{\text{negative}}} \times 100\% \quad (1)$$

2.2.5. Cytotoxicity Test

MCF-7 cells were used to evaluate the cytotoxicity of the samples. MCF-7 cells were cultured in the medium consisting of DMEM/F12 (Paneco, RF, Tokyo, Japan) supplemented with 10% fetal bovine serum (FBS), antibiotics (100 U/mL of penicillin and 100 mg/mL of streptomycin), and 2 mM L-glutamine at 37 °C in a 5% CO₂ and humid atmosphere. The cytotoxicity tests were carried out by direct contact. The control groups involved the use of DMEM as negative controls and 0.64% phenol DMEM as positive controls. Cells were incubated for 24–72 h in 12-well cell culture plates with medium in each well. Next, MTT was added to each well. The samples were incubated with MTT for 4 h at 37 °C, the plates were centrifuged for 10 min at 1500 rpm, the supernatant was carefully removed, and formazan solubilization solution (10% SDS in 0.01 M HCl) was added to each well. The spectrophotometric absorbance of the samples was measured at 540 nm on a Uniplan spectrophotometer (Pikon Inc., RF) with a reference wavelength of 630 nm.

3. Results and Discussion

3.1. XRD Analysis of the NiTi Surfaces

XRD studies have shown that the NiTi25 control sample contains intermetallic phases of the binary system Ti–Ni: NiTi, Ti₂Ni, NiTi₃ and Ti₃Ni₄ at a depth of up to 500 nm from the surface (Figure 2). After annealing at 500 °C, the titanium oxide phase TiO forms on the surface. The qualitative composition of NiTi600 does not differ from the NiTi500 sample, but the quantitative content of the identified phases changed, since the intensity of reflections from the TiO phase increased, and from the intermetallic phases (Ti₂Ni, Ti₃Ni₄) decreased. An increase in the annealing temperature stimulates the segregation of titanium ions from the matrix to the surface, where they form titanium oxides of various oxidation states [24,27,34]. COD and Materials Project databases IDs of the identified phases are presented in Table 1.

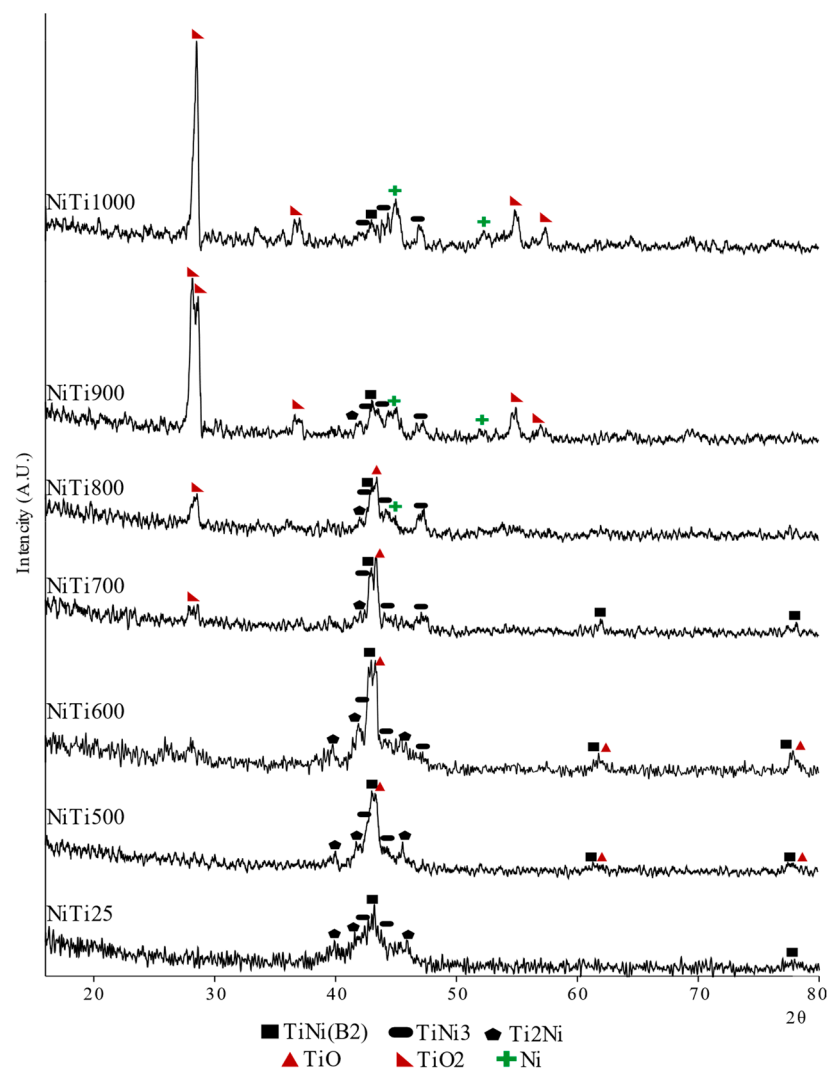


Figure 2. XRD diffractograms of the porous NiTi samples.

Table 1. COD and Materials Project IDs of the identified phases.

Database	NiTi (B2)	Ti ₂ Ni	Ni ₃ Ti	TiO	TiO ₂	Ni
COD ID	mp-23	1527848	1010452	1100042	1530150 tetragonal	1512526
Materials Project ID	mp-571	mp-1808	mp-1409	mp-2664	mp-2657 tetragonal; mp-554278 monoclinic	mp-23

At the annealing temperature of 700 °C, the first crystals of titanium oxide TiO₂ were formed in the rutile modification. At the same time, there was a significant decrease in the intensity of reflections from intermetallic compounds of the Ti–Ni system and from TiO. The TiO₂ oxide in the rutile modification is stable at high temperatures, in contrast to the metastable modifications of brookite and anatase [37]. For samples annealed at higher temperatures compared to the NiTi700 sample, the intensity and number of structural reflections from the TiO₂ phase increased significantly, which indicates an increase in the quantitative content of this phase. NiTi900 has two peaks of TiO₂ indicated at 27–28°. It can be related to the different crystal systems: the first peak is TiO₂ with a monoclinic crystal system and the second one is TiO₂ with a tetragonal crystal system. Free nickel was found in the surface regions of NiTi800, NiTi900, and NiTi1000 samples. Moreover, the intensity and number of Ni structural reflections were found to increase with an increase in the annealing temperature. Ni ions are insoluble in the TiO₂ phase [33]. Therefore, we assume

that nickel did not come to the surface, but was concentrated under a layer of titanium oxides. All 2θ standard angles and Miller indices are presented in Table 2.

Table 2. Standard 2θ angles and Miller indices of the identified phases.

	NiTi (B2)	Ti ₂ Ni	Ni ₃ Ti	TiO	TiO ₂	Ni
2θ standard	42.721	39.141	42.382	42.134	Tetragonal 27.1	
	62.009	41.622	43.556	61.108	35.877	44.776
	78.23	45.509	46.603	77.012	53.793	52.182
					55.886	
					Monoclinic 27.466	
Miller indices	(110)	(422)	(20 $\bar{2}$ 1)	(200)	Tetragonal (110)	
	(200)	(511)	(0004)	(220)	(101)	(111)
	(211)	(440)	(20 $\bar{2}$ 2)	(222)	(211)	(200)
					(220)	
					Monoclinic (11 $\bar{1}$)	

Thus, the oxidation mechanism occurring while annealing the porous NiTi is the same as in the case of the cast NiTi studied by the other authors [28,30–32]. Identical phases form in the area close to the surface and the area consists mostly of TiO₂, if the samples annealed at 900 °C and 1000 °C are concerned.

3.2. SEM and EDS Investigations of the NiTi Surfaces

Images of the pore surface and the flat surface of the samples obtained by optical microscopy and SEM are combined in Figure 3. In NiTi800, NiTi900, NiTi1000 samples, an oxidized white layer was found on the pore surface, which is absent in NiTi25 and NiTi500 samples. Visually, its amount increases with an increase in the annealing temperature from 800 °C to 1000 °C. With an increase in the annealing temperature, the volume fraction of titanium oxides on the surface increases as well.

The temperature dependence of the weight fractions of the elements Ti, Ni and O₂ on the polished surface before annealing is presented in the form of a graph in Figure 4. The polished surface of NiTi25 consists almost entirely of titanium and nickel, found in equal proportions. Furthermore, 8 wt.% oxygen was found in the surface, which can be explained by the presence of adsorbed oxygen. With the growth of the annealing temperature, the Ni content decreases because titanium ions have a better affinity to oxygen. Ti ions segregate to the surface during annealing, where they form titanium oxide. This oxide layer becomes thicker with the increase in the annealing temperature so the growth of Ti and O₂ weight fraction can be seen. The decrease in the Ni content on the surface of the oxidized alloy at temperatures of 600–900 °C is due to the growth of titanium oxides on the outer surface of the porous framework which cover the underlying layers containing nickel.

Figure 5 shows crystals found on the pore surface of samples annealed at temperatures above 700 °C. The shape of the crystals in the NiTi700 sample is predominantly filamentary, while in the NiTi900 sample the crystals have a needle shape. In accordance with the studies by the other authors, these crystals are the TiO₂ phase [38], which fully confirms the XRD data, according to which the content of the TiO₂ phase increases with the increase in the annealing temperature.

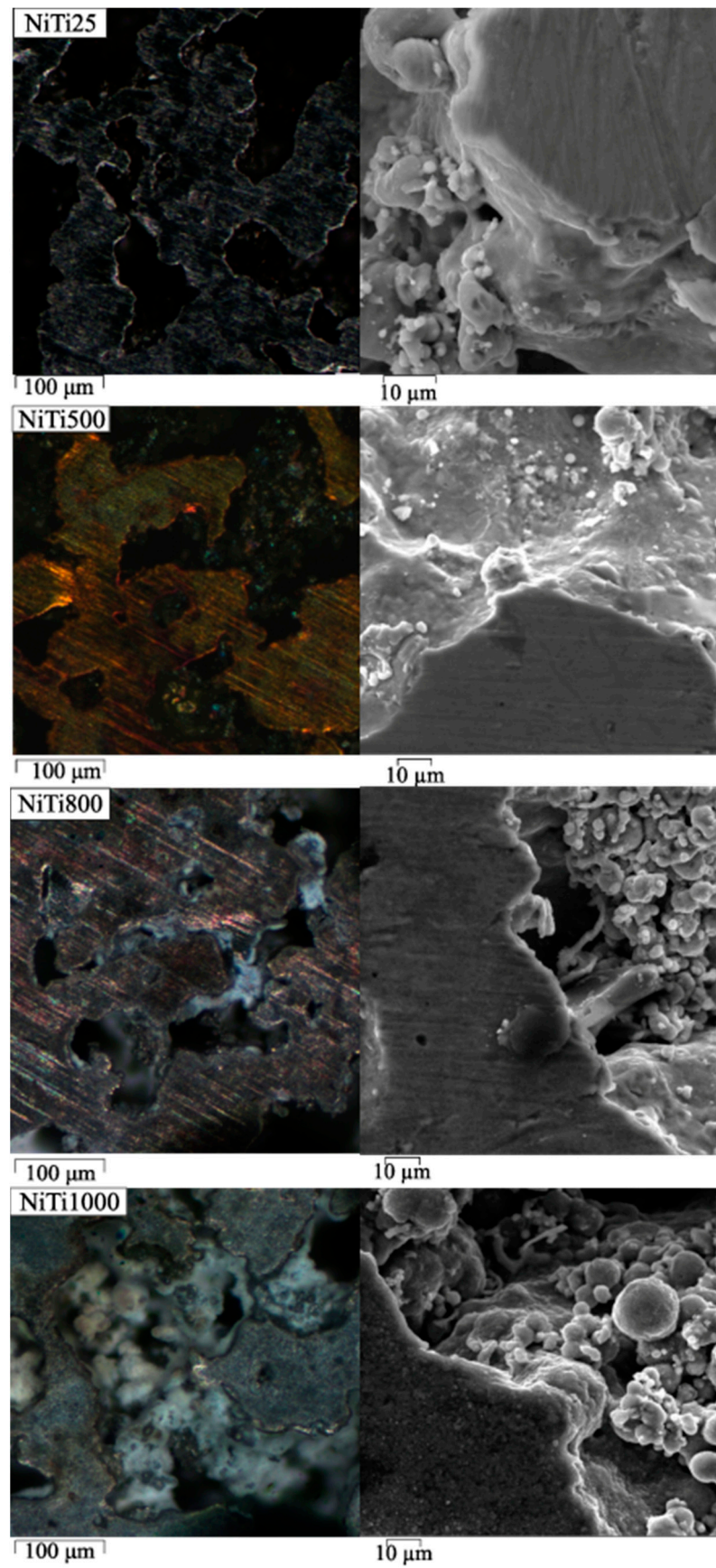


Figure 3. Optical and SEM microscopy images of surfaces of NiTi porous samples.

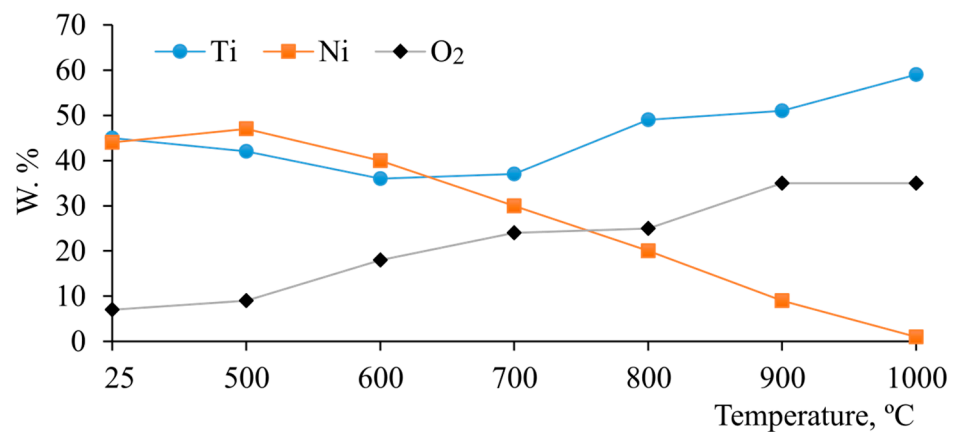


Figure 4. The elements weight fraction dependence on annealing temperatures.

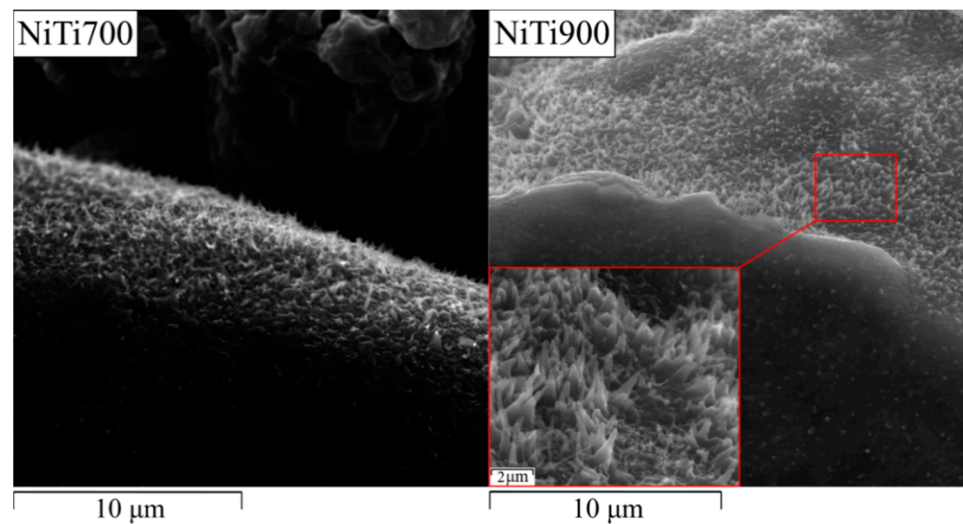


Figure 5. SEM crystals images grown up on the pore surfaces of the annealed samples.

3.3. Ni Content in Solution and Hemolysis Test

Before culturing the cells, the intensity of nickel release during the dissolution of oxidized porous NiTi samples was studied, since the concentration of nickel in solutions becomes toxic as it reaches its maximum allowed amount [39]. The data available in existing literature show that NiTi alloys corrode in biological solutions and a certain precipitate appears when nickel is dissolved [40]. At the early stages of the experiment (after 100 h) the appearance of the green color trace of 1% mass. HCl solution was detected, which points at the dissolution of nickel ions. At the later stages (after 860 h) a light precipitate of unknown composition appeared. The nickel release content in annealed porous samples when dissolved in a 1 mass. % HCl solution for 1800 h is shown in Figure 6a.

The NiTi500 sample has a nickel ion concentration of 0.9 mg/L, which is 0.35 mg/L higher than that of NiTi25. Heating to 600 °C and 700 °C increases the release of nickel ions into the solution to 0.85 and 0.8 mg/L, respectively, compared to NiTi25. Heating NiTi to temperatures in the range of 800–1000 °C made it possible to reduce the concentration of leached nickel in a 1 mass. % HCl. For NiTi800, NiTi900 and NiTi1000, nickel ion concentrations of 0.45, 0.34, and 0.33 mg/L were observed, which is much lower compared to NiTi25. Annealing of porous NiTi alloys in air at a temperature of 800–1000 °C leads to the formation of an oxide layer on the surface of the pores, which successfully prevents the nickel release to the surface. This agrees with the studies of other authors [26–28,31–35].

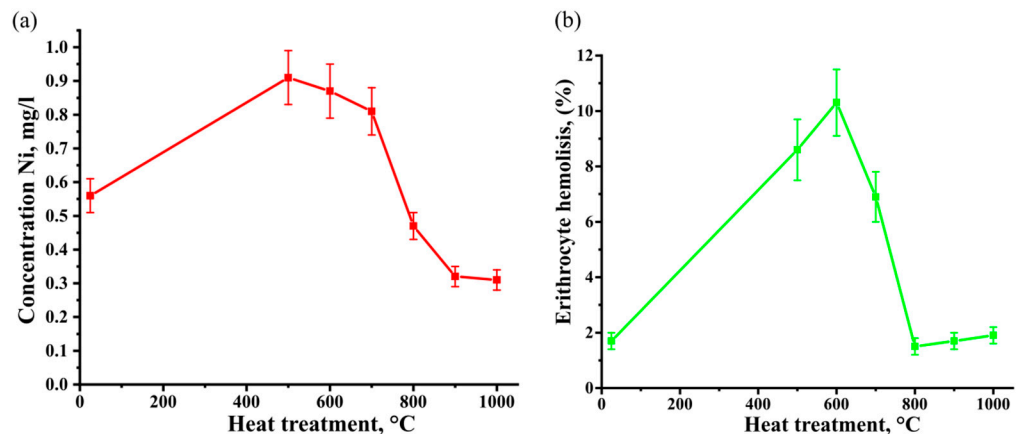


Figure 6. (a) The concentration of nickel accumulated in the solution is 1 macc. % HCl as a result of corrosion of porous heat treated NiTi-alloys samples for 1800 h (red line), (b) hemolysis percentage of porous heat treated NiTi-alloys samples (green line).

RBC hemolysis on porous NiTi alloy samples after heat treatment is shown in Figure 6b. A non-linear nature of the change in the hemolytic index is observed, while for the control sample it is $1.7 \pm 0.3\%$, for NiTi500— $8.6 \pm 1.1\%$, for NiTi600— $10.3 \pm 1.2\%$ and for NiTi700— $6.9 \pm 0.9\%$. These parameters exceed the allowed values of about 2% according to ISO 10993-4:2018 for hemolysis by biomaterials in contact with blood, which indicates the unsuitability of these heat treatment modes. For NiTi800 alloys— $1.5 \pm 0.3\%$, for NiTi900— $1.7 \pm 0.3\%$, for NiTi1000— $1.9 \pm 0.3\%$ (Figure 6b). The hemolysis index of samples with an annealing temperature in the range of 800–1000 °C is significantly lower than 500–700 °C and falls within the allowed range of ISO 10993-4:2018 standard up to 2%.

3.4. Cytotoxicity Test

MCF-7 cells were incubated for 24 h on heat-treated porous NiTi samples and evaluated by MTT assay in static culture. Figure 6 shows the comparison of morphological images of MCF-7 cells on porous NiTi alloy samples annealed at temperatures of 500–1000 °C. Local surface areas with MCF-7 cells were found on the control sample, where live cells are shown in green with red nuclei.

A high level of cytotoxicity equal to $61 \pm 7\%$ in relation to MCF-7 cells was found on the NiTi500 sample, which is higher than that on the control NiTi25 sample (Figure 7). The highest level of cytotoxicity was found on the NiTi600 sample, where it was $74 \pm 7\%$. On the NiTi700 sample, the level of cytotoxicity was $58 \pm 6\%$. A low level of cytotoxicity towards MCF-7 cells was found on NiTi800, NiTi900, and NiTi1000 samples, where it was $14 \pm 7\%$, $21 \pm 4\%$, and $28 \pm 4\%$, respectively.

In the image of the NiTi500 sample, a large number of cells stained red as a result of the release of chromatin from the nucleus and its staining with ethidium bromide can be seen, which indicates a sharp decrease in the level of cell viability. At the same time, no living cells stained green with acridine orange are on the surface of this sample. This fact indicates the death of cells within 72 h after their attachment to the surface of the NiTi500 sample due to cytotoxic factors present on the surface of the sample.

In the image of NiTi600 and NiTi700 samples, a small number of viable green cells attached to the surface and a large number of non-viable cells stained in yellow and red are found. The nickel content on the surface is positively correlated with the level of cytotoxicity. The level of cytotoxicity decreases as the outer layers of titanium oxide grow. The growth of cytotoxicity index after annealing at 500–700 °C can be related to the TiO formation because Ni can be freely dissolved in TiO [33] and provides a negative influence on viable cells, which results in bad proliferation ability and further cell's mortification (red cells).

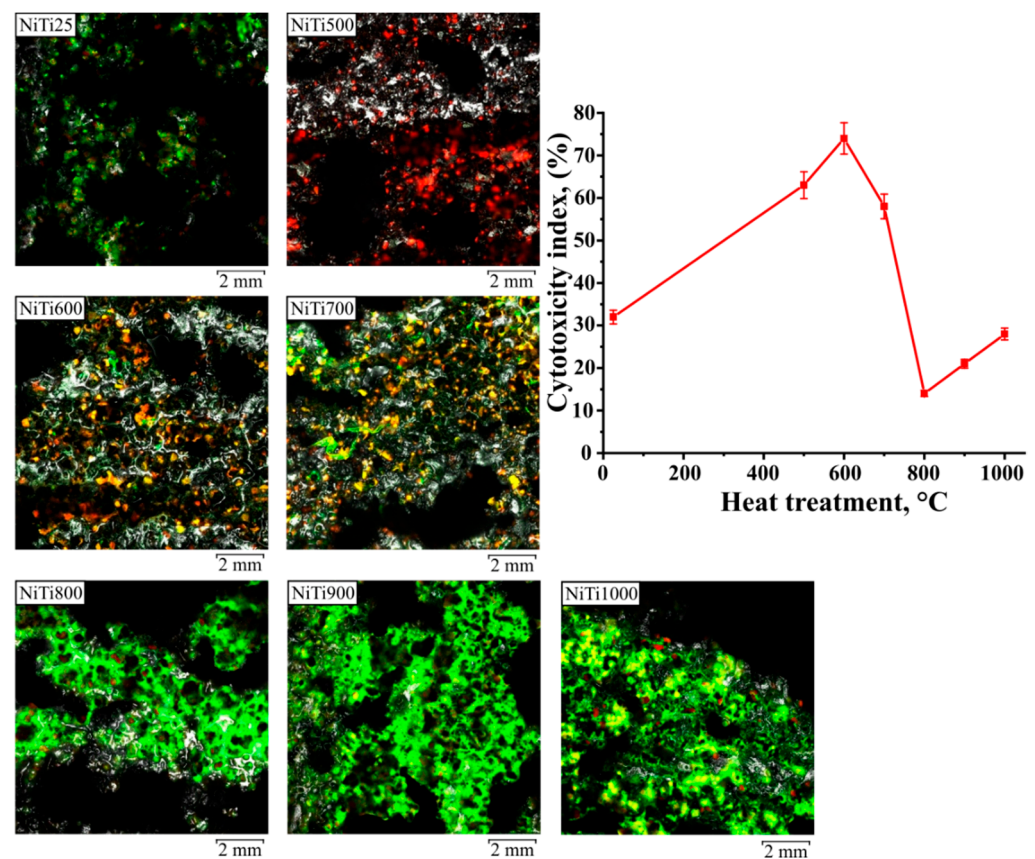


Figure 7. CLSM images of various samples of NiTi after cell growth MCF-7 for 3 days, green color used for visualization of viable MCF-7 cells; cytotoxicity level of the modified porous NiTi-based alloy samples with MCF-7 cells after 24 h of incubation, measured by the MTT test (red line).

The images confirm that the area occupied by green-colored cells attached to the surface of the sample significantly increased in the samples annealed at temperatures of 800–1000 °C. The cells show numerous cytoplasmic structures and many of them have a proliferative morphology.

Using confocal microscopy, similar changes were found in terms of cytocompatibility with MCF-7 cells. Based on these data, it can be concluded that in static culture, MCF-7 cells seeded on the control and heat-treated samples at a temperature of 800–1000 °C had the highest proliferative activity.

In this work, the cytocompatibility control method fully correlates with the results obtained by XRD, SEM, confocal and optical microscopy. We can conclude that the annealing of porous NiTi alloy implants at 500–700 °C is not recommended because it leads to a worse cell proliferation and high corrosion level. The recommended annealing temperatures are 800–1000 °C because the samples heat-treated at these temperatures demonstrate the highest corrosion resistance level, the highest cell proliferation ability and the greatest number of the surviving cells.

4. Conclusions

To conclude, short-time annealing of porous NiTi in the temperature range of 500–1000 °C causes changes in the surface phase composition. The weight fractions of the intermetallic phases such as NiTi B2, Ti₂Ni, TiNi₃ decrease along with an increase in the annealing temperature, but at the same time new phases such as TiO, TiO₂ and Ni form due to Ti ion segregation to the surface. An increase in the yield of nickel into the chlorine-containing solution after short-time annealing from 500 to 700 °C is observed. At the same time, short-time annealing from 800 to 1000 °C reduced the concentration of leached nickel in the solution. This can be related to TiO₂ formation because this phase acts as a protective

barrier against biological liquid tissues. These data directly correlate with the percentage of erythrocyte hemolysis, the cytotoxicity index, and the number of detected cells. After annealing at 800–1000 °C, a decrease in the percentage of hemolysis to normal values, a decrease in the cytotoxic activity of porous samples, and an increase in the viability of cell cultures were established.

Further investigation will be focused on the mechanical properties and martensitic transformation of the annealed porous SHS-TiNi samples.

Author Contributions: Conceptualization, E.M., G.B. and Y.Y.; methodology, E.M. and O.K.; validation, E.M., G.B. and Y.Y.; formal analysis, K.D. and O.K.; resources, K.D. and O.K.; writing—original draft preparation, K.D. and O.K.; writing—review and editing, K.D., O.K. and G.B.; visualisation, K.D.; supervision, E.M. and Y.Y.; project administration, G.B.; funding acquisition, E.M. and A.V. All authors have read and agreed to the published version of the manuscript.

Funding: This study was supported by the Tomsk State University Development Programme (Priority-2030).

Institutional Review Board Statement: The study was conducted in accordance with the Declaration of Helsinki and approved by Bioethical Committee of Tomsk State (approval protocol code number No 20/1116/2017).

Informed Consent Statement: Informed consent was obtained from all subjects involved in the study.

Data Availability Statement: Not applicable.

Acknowledgments: The structure research was carried out with the equipment of Tomsk Regional Core Shared Research Facilities Center of National Research Tomsk State University (Grant of the Ministry of Science and Higher Education of the Russian Federation no. 075-15-2021-693 (no. 13.RFC.21.0012)).

Conflicts of Interest: The authors alone are responsible for the content and declare that there is no conflict of interest. The authors have no financial interest in the products presented in this report.

References

1. Dong, B.; Wu, F.; Alajmi, Z.; Zhang, C.; Fu, T.; Ge, Y. Sol-gel derived Ta-containing TiO₂ films on surface roughened NiTi alloy. *Rare Met.* **2014**, *33*, 21–27. [[CrossRef](#)]
2. Tao, F.; Hongwei, L.; Feng, W.; Wen, L.; Jianmin, S. One-Step Synthesis of TiO₂-Hydroxyapatite Nano-films on NiTi Alloy by Hydrothermal Method. *Rare Met. Mater. Eng.* **2016**, *45*, 1128–1131. [[CrossRef](#)]
3. Jani, J.M.; Leary, M.; Subic, A.; Gibson, M.A. A review of shape memory alloy research, applications and opportunities. *Mater. Des.* **2014**, *56*, 1078–1113. [[CrossRef](#)]
4. Zhang, L.; Zhang, Y.; Jiang, Y.; Zhou, R. Superelastic behaviors of biomedical porous NiTi alloy with high porosity and large pore size prepared by spark plasma sintering. *J. Alloys Compd.* **2015**, *644*, 513–522. [[CrossRef](#)]
5. Gunther, V.E.; Yasenchuk, Y.; Gyunter, S.V.; Marchenko, E.S.; Iuzhakov, M.M. Biocompatibility of porous SHS-TiNi. *Mater. Sci. Forum* **2019**, *970*, 320–327. [[CrossRef](#)]
6. Dotter, C.T.; Buschmann, P.C.; McKinney, M.K.; Rosch, J. Transluminal expandable nitinol coil stent grafting: Preliminary report. *Radiology* **1983**, *147*, 259–260. [[CrossRef](#)] [[PubMed](#)]
7. Stoeckel, D. Nitinol medical devices and implants. *Minim. Invasive Ther. Allied Technol.* **2000**, *9*, 81–88. [[CrossRef](#)]
8. Duerig, T.W.; Tolomeo, D.E.; Wholey, M. An overview of superelastic stent design. *Minim. Invasive Ther. Allied Technol.* **2000**, *9*, 235–246. [[CrossRef](#)]
9. Čapek, J.; Vojtěch, D. Powder metallurgical techniques for preparation of biomaterials. *Manuf. Technol.* **2015**, *15*, 964–969. [[CrossRef](#)]
10. Mediaswanti, K.; Wen, C.; Ivanova, E.; Berndt, C.; Malherbe, F.; Pham, V.; Wang, J. A Review on Bioactive Porous Metallic Biomaterials. *J. Biomim. Biomater. Tissue Eng.* **2013**, *18*, 2–8. [[CrossRef](#)]
11. Hu, T.; Chu, C.; Xin, Y.; Wu, S.; Yeung, K.; Chu, P. Corrosion products and mechanism on NiTi shape memory alloy in physiological environment. *J. Mater. Res.* **2010**, *25*, 350–358. [[CrossRef](#)]
12. Marchenko, E.S.; Yasenchuk, Y.; Gyunter, S.V.; Bajgonakova, G.A.; Gunther, V.E.; Chekalkin, T.L.; Weiss, S.; Obrosof, A.; Dubovikov, K.M. Structural-phase surface composition of porous NiTi produced by SHS. *Mater. Res. Express.* **2019**, *6*, 1165–1175. [[CrossRef](#)]
13. Yasenchuk, Y.F.; Gunther, V.E.; Marchenko, E.S.; Chekalkin, T.L.; Bajgonakova, G.A.; Khodorenko, V.N.; Gyunter, S.V.; Kang, J.H.; Weiss, S.; Obrosof, A. Formation of mineral phases in self-propagating high-temperature synthesis (SHS) of porous NiTi alloy. *Mater. Res. Express.* **2019**, *6*, 056522. [[CrossRef](#)]

14. Kokorev, O.V.; Khodorenko, V.N.; Baigonakova, G.A.; Marchenko, E.S.; Yasenchuk, Y.; Gunther, V.E.; Anikeev, S.G.; Barashkova, G.A. Metal-Glass-Ceramic Phases on the Surface of Porous NiTi-Based SHS-Material for Carriers of Cells. *Russ. Phys. J.* **2019**, *61*, 1734–1738. [[CrossRef](#)]
15. Lou, J.; He, H.; Li, Y.; Zhu, C.; Chen, Z.; Liu, C. Effects of high O contents on the microstructure, phase-transformation behaviour, and shape-recovery properties of porous NiTi-based shape-memory alloys. *Mater. Des.* **2016**, *106*, 37–44. [[CrossRef](#)]
16. Yasenchuk, Y.; Marchenko, E.; Gunther, V.; Radkevich, A.; Kokorev, O.; Gunther, S.; Baigonakova, G.; Hodorenko, V.; Chekalkin, T.; Kang, J.; et al. Biocompatibility and Clinical Application of Porous TiNi Alloys Made by Self-Propagating High-Temperature Synthesis (SHS). *Materials* **2019**, *12*, 2405. [[CrossRef](#)]
17. Petruk, P.S.; Medvedev, Y.A.; Show, Y.Z.; Volkova, V.A. Nickel-Titanium Shape Memory Alloy in Reconstructive Osteosynthesis in Patients with Zygomatico-Orbital Complex Fractures. SMBIM Conference Proceedings Shape Memory Biomaterials and Implants in Medicine. *KnE Mater. Sci.* **2017**, *2017*, 323–326. [[CrossRef](#)]
18. Radkevich, A.A.; Gantimurov, A.A.; Gunther, V.E.; Platonova, N.V. Replacement of Temporomandibular Joint Head Using the Shape Memory Materials. SMBIM Conference Proceedings Shape Memory Biomaterials and Implants in Medicine. *KnE Mater. Sci.* **2017**, *2017*, 184–192. [[CrossRef](#)]
19. Medvedev, Y.A.; Basin, E.M.; Milyukova, D.Y. Mandibular TiNi-based Endograft in Patients with Toxic Jaw Osteonecrosis and Drug Abuse. SMBIM Conference Proceedings Shape Memory Biomaterials and Implants in Medicine. *KnE Mater. Sci.* **2017**, *2017*, 280–285. [[CrossRef](#)]
20. Ammarullah, M.I.; Afif, I.Y.; Maula, M.I.; Winarni, T.I.; Tauviqirrahman, M.; Akbar, I.; Basri, H.; van der Heide, E.; Jamari, J. Tresca Stress Simulation of Metal-on-Metal Total Hip Arthroplasty during Normal Walking Activity. *Materials* **2021**, *14*, 7554. [[CrossRef](#)]
21. Jamari, J.; Ammarullah, M.I.; Saad, A.P.M.; Syahrom, A.; Uddin, M.; van der Heide, E.; Basri, H. The Effect of Bottom Profile Dimples on the Femoral Head on Wear in Metal-on-Metal Total Hip Arthroplasty. *J. Funct. Biomater.* **2021**, *12*, 38. [[CrossRef](#)] [[PubMed](#)]
22. Zou, J.X.; Grosdidier, T.; Zhang, K.M.; Dong, C.; Weber, S. Mechanism of surface modifications on a NiTi alloy treated with low energy high current pulsed electron beam. *EPJ Appl. Phys.* **2008**, *43*, 327–331. [[CrossRef](#)]
23. Ponsonnet, L.; Reybier, K.; Jaffrezic, N.; Comte, V.; Lagneau, C.; Lissac, M.; Martelet, C. Relationship between surface properties (roughness, wettability) of titanium and titanium alloys and cell behavior. *Mater. Sci. Eng. C* **2003**, *23*, 551–560. [[CrossRef](#)]
24. Hansen, A.W.; Beltrami, L.V.R.; Antonini, L.M.; Villarinho, D.J.; das Neves, J.C.K.; Marino, C.E.B.; Malfatti, C.F. Oxide Formation on NiTi Surface: Influence of the heat Treatment Time to Achieve the Shape Memory. *Mater. Res.* **2015**, *18*, 1053–1061. [[CrossRef](#)]
25. Ferraris, S.; Cazzola, M.; Peretti, V.; Stella, B.; Spriano, S. Zeta potential measurements on solid surfaces for in vitro biomaterials testing: Surface charge, reactivity upon contact with fluids and protein absorption. *Front. Bioeng. Biotechnol.* **2018**, *6*, 60–67. [[CrossRef](#)]
26. Mahmud, A.; Wu, Z.; Zhang, J.; Liu, Y.; Yang, H. Surface oxidation of NiTi and its effects on thermal and mechanical properties. *Intermetallics* **2018**, *103*, 52–62. [[CrossRef](#)]
27. Gu, Y.W.; Tay, B.Y.; Lim, C.S.; Yong, M.S. Characterization of bioactive surface oxidation layer on NiTi alloy. *Appl. Surf. Sci.* **2005**, *252*, 2038–2049. [[CrossRef](#)]
28. Chu, C.L.; Wu, S.K.; Yen, Y.C. Oxidation behavior of equiatomic NiTi alloy in high temperature air environment. *Mater. Sci. Eng. A* **1996**, *216*, 193–200. [[CrossRef](#)]
29. Dagdelen, F.; Ercan, E. The surface oxidation behavior of Ni–45.16%Ti shape memory alloys at different temperatures. *J. Therm. Anal. Calorim.* **2014**, *115*, 561–565. [[CrossRef](#)]
30. Liu, X.; Wang, Y.; Yang, D.; Qi, M. The effect of ageing treatment on shape-setting and superelasticity of a nitinol stent. *Mater. Charact.* **2008**, *59*, 402–406. [[CrossRef](#)]
31. Shabalovskaya, S.; Anderegg, J.; Humbeeck, J. Critical overview of Nitinol surfaces and their modifications for medical applications. *Acta Biomater.* **2008**, *4*, 447–467. [[CrossRef](#)] [[PubMed](#)]
32. Firstov, G.S.; Vitchev, R.G.; Kumar, H.; Blanpain, B.; Van Humbeeck, J. Surface oxidation of NiTi shape memory alloy. *Biomaterials* **2002**, *23*, 4863–4871. [[CrossRef](#)]
33. Tian, H.; Schryvers, D.; Liu, D.; Jiang, Q.; Van Humbeeck, J. Stability of Ni in nitinol oxide surfaces. *Acta Biomater.* **2011**, *7*, 892–899. [[CrossRef](#)]
34. Undisz, A.; Schrempel, F.; Wesch, W.; Rettenmayr, M. Mechanism of oxide layer growth during annealing of NiTi. *J. Biomed. Mater. Res. A* **2012**, *100*, 1743–1750. [[CrossRef](#)] [[PubMed](#)]
35. Huang, J.; Dong, P.; Hao, W.; Wang, T.; Xia, Y.; Da, G.; Fan, Y. Biocompatibility of TiO₂ and TiO₂/heparin coatings on NiTi alloy. *Appl. Surf. Sci.* **2014**, *313*, 172–182. [[CrossRef](#)]
36. Gunther, V.; Yasenchuk, Y.; Chekalkin, T.; Marchenko, E.; Gunther, S.; Baigonakova, G.; Hodorenko, V.; Kang, J.H.; Weiss, S.; Obrosova, A. Formation of pores and amorphous nanocrystalline phases in porous NiTi alloys made by self-propagating high-temperature synthesis (SHS). *Adv. Powder Technol.* **2019**, *30*, 673–680. [[CrossRef](#)]
37. Diebold, U. The surface science of titanium dioxide. *Surf. Sci. Rep.* **2003**, *48*, 53–229. [[CrossRef](#)]
38. Weng, C.; Chen, C.; Ting, C.; Wei, K. Using a solution crystal growth method to grow arrays of aligned, individually distinct, single-crystalline TiO₂ nanoneedles within nanocavities. *Chem. Mater.* **2005**, *17*, 3328–3330. [[CrossRef](#)]

-
39. Blanco-Dalmau, L.; Carrasquillo-Alberty, D.; Silva-Parra, J. A study of nickel allergy. *J. Prosthet. Dent.* **1984**, *52*, 116–119. [[CrossRef](#)]
 40. Shabolovskaya, S.A. Surface, corrosion and biocompatibility aspects of Nitinol as an implant material. *Biomed. Mater. Eng.* **2002**, *12*, 69–109.